Electronic Supplementary Material (ESI) for Journal of Materials Chemistry C.

One-pot in-situ Synthesis of $CsPbX_3$@h-BN (X = Cl, Br, I) Nanosheet Composites with Superior Thermal Stability for White LEDs

Lei Qiu, [# a] Jiarui Hao, [# a] Yuxin Feng, [a] Xingyu Qu, [a] Guogang Li, * [a] Yi Wei, [a] Gongcheng Xing, [a] Hongquan Wang, [a] Chunjie Yan *[a] and Jun Lin *[b, c]

[a.] *Engineering Research Center of Nano-Geomaterials of Ministry of Education, Faculty of Materials Science and Chemistry, China University of Geosciences, 388 Lumo Road, Wuhan 430074, P. R. China.*

[b.] *State Key Laboratory of Rare Earth Resource Utilization, Changchun Institute of Applied Chemistry, Chinese Academy of Sciences, Changchun 130022, P. R. China.*

[c.] *School of Applied Physics and Materials, Wuyi University, Jiangmen, Guangdong 529020, P. R. China*

Abstract: All-inorganic lead perovskite nanocrystals (NCs) are very susceptible to heat and thus easily suffer thermal quenching, which severely hinder their practical applications in opto-electronic devices. In this work, one-pot in-situ strategy is adopted to directly grow uniform perovskite nanocrystals on exfoliated two-dimension (2D) hexagonal boron nitride nanosheets (h-BN NSs). Such a nanohybrid structure shows excellent thermal conductivity, and it could timely dissipate the excess heat. As a consequence, superior thermal stability is achieved, which the photoluminescence emission intensity at 120°C still maintains 80% of initial intensity at 25°C (nearly 6 times of pure perovskite NCs). This result presents the highest thermal stability ever reported in inorganic composites based on all inorganic lead halide perovskite materials, which provides a new opportunity for $CsPbX_3$ (X = Cl, Br, I) NCs to find promising applications in perovskite NCs-based opto-electronic devices such as white light emitting diodes (LED) devices.

Experimental Procedures

Materials: Cesium carbonate (Cs_2CO_3, 99.5%, Acros organics), lead(II) iodide (PbI_2, 99.99%, Aladdin), lead(II) bromide ($PbBr_2$, 99.999%, Aladdin), lead(II) chloride ($PbCl_2$, 99.999%, Sigma), oleic acid (OA, technical grade 90%, Aldrich), oleylamine (OAm, 80~90%, Aladdin), 1-octadecene (ODE, > 90%, Aladdin), hexane (analytical reagent 97%, Sinopharm Chemical Reagent Co., Ltd. (Shanghai)), ethyl acetate (Sinopharm Chemical Reagent Co., Ltd. (Shanghai)), urea (≥ 99%, Sinopharm Chemical Reagent Co., Ltd. (Shanghai)) and hexagonal boron nitride (h-BN, 99.5%, Aladdin). All the chemicals except for h-BN in this work were used without further treatment.

Exfoliation of h-BN NSs: The purchased h-BN was exfoliated through a modified ball milling method with the assistance of urea. In brief, the pristine h-BN (1.00g), urea (60.00g) and deionized water (20.00 ml) were homogeneously mixed into a steel milling container using a planetary ball mill at a low rotation speed of 90 rpm/min for 30 h at room temperature in atmospheric environment. After ball milling, the mixture was dried in vacuum drying oven over night and then was calcined in a muffle furnace at 500 ^oC for 10 h in air. Under the same exfoliated conditions, the h-BN was also treated at different rotation time such as 10 h, 20 h, 40 h and 60 h. All exfoliated h-BN NSs were reserved in centrifuge tubes for further use.

Synthesis of Cs-Oleate: In a typical experiment, Cs_2CO_3 (0.8140 g), OA (5.00 mL), and ODE (50.00 mL) were loaded into a 100 mL three-necked flask and stirred under vacuum for 1 h at 120^oC. Then, the solution was heated at 150^oC under N_2 until it became clear and transparent, implying the complete reaction of Cs_2CO_3 and OA. The Cs-Oleate solution was stored under N_2 and needed to be preheated to 100 ^oC before further use because it would precipitate at room temperature.

Synthesis of $CsPbX_3$@h-BN composite powders: Using the green-emitting $CsPbBr_3$ NCs as an example, the $CsPbX_3$@h-BN composite was synthesized *via* a typical hot-injection method. Generally, $PbBr_2$ (0.94 mmol, 0.3450 g), ODE (25.00 mL), OA (2.50 mL), OAm (2.50 mL) and BN-E (0.1000 g) were one-pot added into a 50 mL three-necked flask, and the mixture was uniformly dispersed by an ultrasonic treatment for 10 mins. Next, the mixture was dried at 120^oC for 1 h under vacuum to guarantee a complete dissolution of $PbBr_2$ and then the temperature was elevated to 180^oC in N_2 atmosphere. When the temperature reached 180^oC, Cs-Oleate (2 mL) was rapidly injected into the flask. The flask was immediately cooled down by an ice bath after the mixture reacted five seconds, and then the $CsPbBr_3$@BN-E colloidal solution was obtained. The above solution was centrifuged at 9000 rpm/min

for 10 min to obtain the resulting $CsPbBr_3$@BN-E composite precipitates. The as-prepared precipitates were then washed with ethyl acetate/toluene hybrid solution (volume ratio = 1:1) and centrifuged for serval times to form the final $CsPbBr_3$@BN-E phosphors. As for different $CsPbBr_3$@BN-E composites, all above procedures remained unchanged except for various types of BN, different connection of BN-E (1.67, 2.67, 3.34, 6.68 and 10.02 mg/mL), diverse ultrasonic treatment time of BN (0 h, 10 h, 20 h, 30 h, 40 h and 60 h), or hybrid halide composites [0.94 mmol PbX_2 (X = Cl, Br, I) in total] were altered one by one. The CPB@BN-U was synthesized by combining pure CPB with exfoliated BN *via* a direct ultrasonic treatment for 10 mins as comparison.

Fabrication of LED devices: 0.025 g of $CsPbBr_3$@BN-E, $CsPbBr_{1.2}Cl_{1.8}$@BN-E and $CsPbBr_{1.2}I_{1.8}$@BN-E composites phosphors were mixed with 0.025 g of silicone resin B. The resulting mixture was then heated to 40 ^oC for 1 h to remove the solvent. Silicone resin A (0.025 g) were mixed with the previously prepared mixture. In order to eliminate air bubbles, the mixture was placed into a vacuum oven for 30 mins at 50 ^oC to form a composite sol. Subsequently, the mixture was dropped onto a 400 nm InGaN near ultraviolet -emitting chip. The electroluminescence properties of the fabricated devices were determined by using an integrating sphere with an analyzer system (Starspec SSP6612) under a voltage of 3.15 V and current of 20 mA.

Characterizations: The crystal structure and phase purity were characterized by X-ray powder diffraction (XRD), which was performed on a D8 Focus diffractometer at as canning rate of 1° min^{-1} in the 2θ range from 10° to 60° with Nifiltered Cu Kα (λ = 1.540598 Å). Fourier transformation infra-red (FTIR) spectra were taken by using a Fourier transformation infra-red spectrometer (Thermo Fisher Scientific, IS50). The morphologies, energy-dispersive X-ray spectrum (EDS) and elemental mapping analysis of the studied samples were inspected using a field emission scanning electron microscope (FE-SEM, S-4800, Hitachi) and Transmission electron microscope (FEI Tecnai G2 F20). The absorption spectra were measured by UV−visible diffuse reflectance spectroscopy UV-2550PC (Shimadzu Corporation, Japan). The photoluminescence spectra were measured by fluorescence spectrometer (Fluoromax-4P, Horiba JobinYvon, New Jersey, U.S.A.) equipped with a 150 W xenon lamp as the excitation source, and both excitation and emission spectra were set up to be 1.0 nm with the width of the monochromator slits adjusted to 0.50 nm. The thermal stability of luminescence properties was measured by Fluoromax-4P spectrometer connected heating equipment (TAP-02) and using a combined setup consisting of a Xe-lamp, a Hamamatsu MPCD-7000 multichannel photodetector and a computer-controlled heater. The photoluminescence quantum yield (QY) was measured by an absolute PL quantum yield measurement system C9920-02 (Hamamatsu photonics K.K., Japan). The photoluminescence decay curves were obtained from a Lecroy Wave Runner 6100 Digital Osilloscope (1 GHz) using a tunable laser

(pulse width = 4 ns, gate = 50 ns) as the excitation (Contimuum Sunlite OPO). Heat conductivity test: The heat conductivity was measured using a thermal conductometer (XIATECH TC30000E) with a heat sensor (9P3000E). The sample was tiled on ground glass with thickness around 1 mm, and heat sensor was clamped between two ground glasses. The test voltage was 1.5 V and test interval was 3 min at room temperature.

Results and Discussion

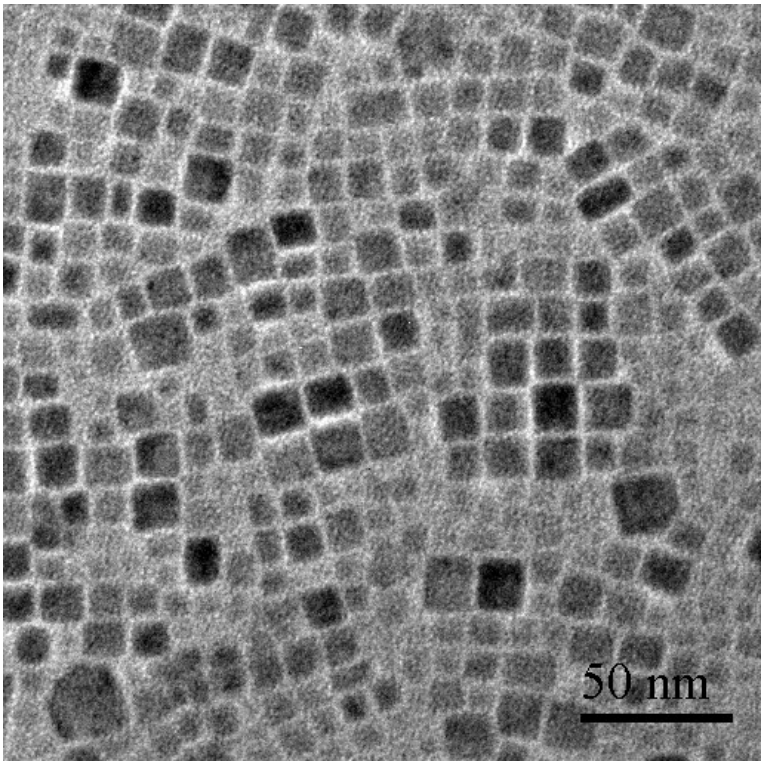

Figure S1. TEM image of CPB after ultrasonic treatment with 1 h.

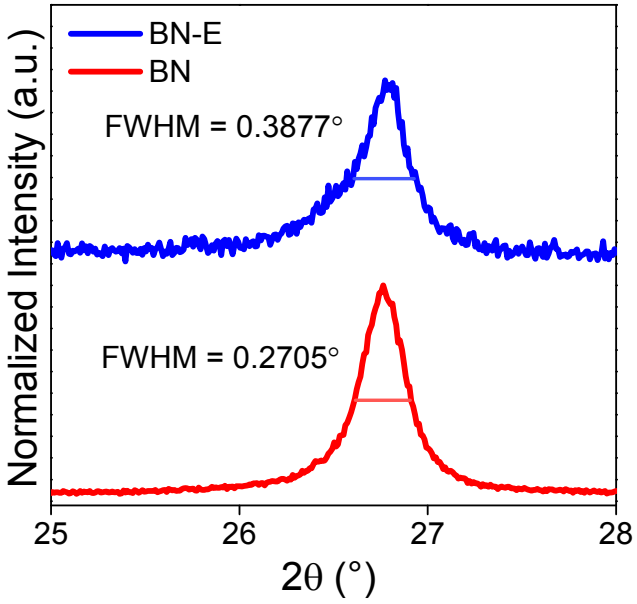

Figure S2. Magnified XRD patterns of BN and BN-E.

As can be seen, the FWHM is changed from 0.2705° to 0.3877° after 30 h of exfoliating and the result proves the widening of h-BN (002) peak. It is worthy that the exfoliated BN (BN-E) or composite CPB@BN-E in manuscript are all corresponding to exfoliating time of 30 h. Since the peak corresponds to the (002) planes, its width is related to the number of diffracting planes in z direction, indicating the BN become thinner. The thickness of BN-E could be roughly calculated by Scherrer Formula: $D = K\lambda/B\cos\theta$, so the thickness is about 20.83 nm. As confirmed by transmission electron microscopy (TEM) and atomic force microscopy (AFM) in reference 1 in supporting information, the thickness of the few-layer BN is about 2 nm (five to six monolayers), so our exfoliated BN-E nano-sheets might be fifty to sixty monolayers.

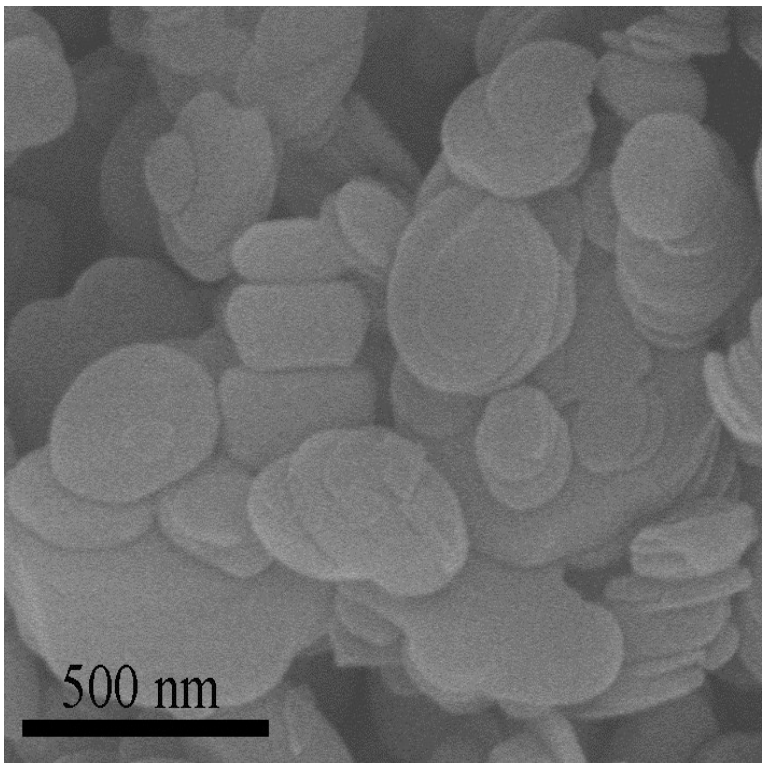

Figure S3. SEM image of pristine BN

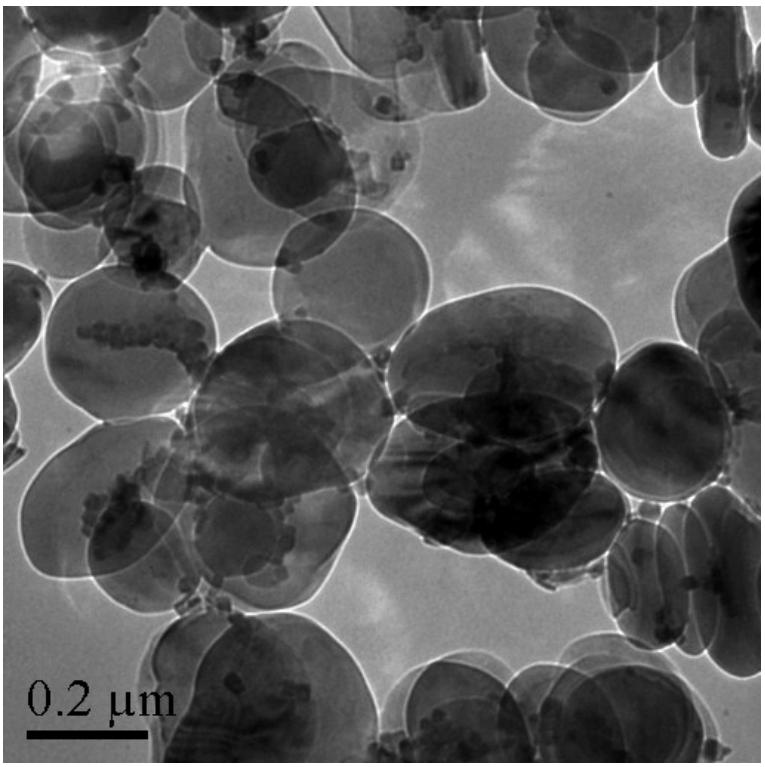

Figure S4. TEM image of CPB@BN after ultrasonic treatment with 1 h.

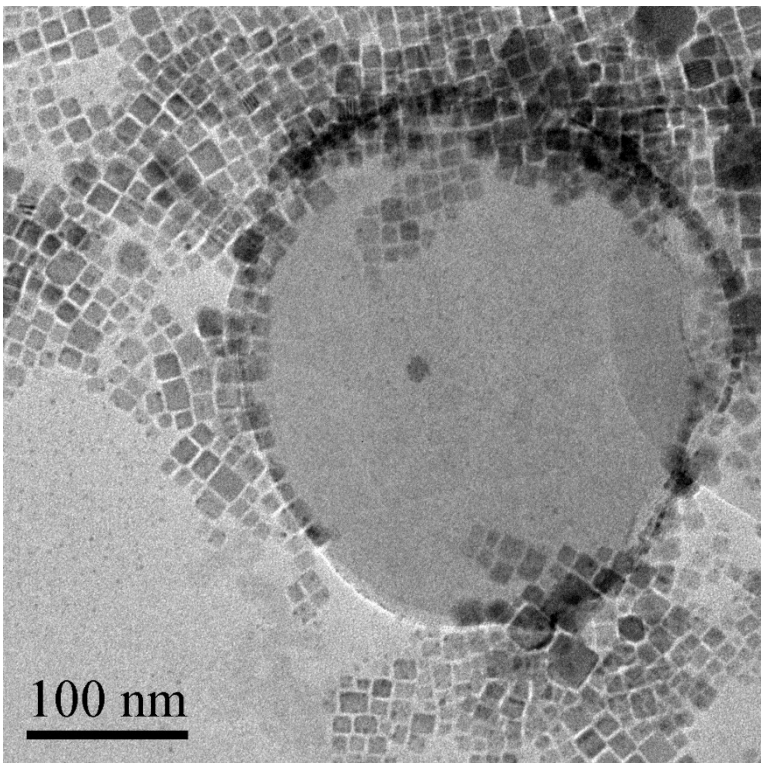

Figure S5. TEM image of CPB@BN-U after ultrasonic treatment with 1 h.

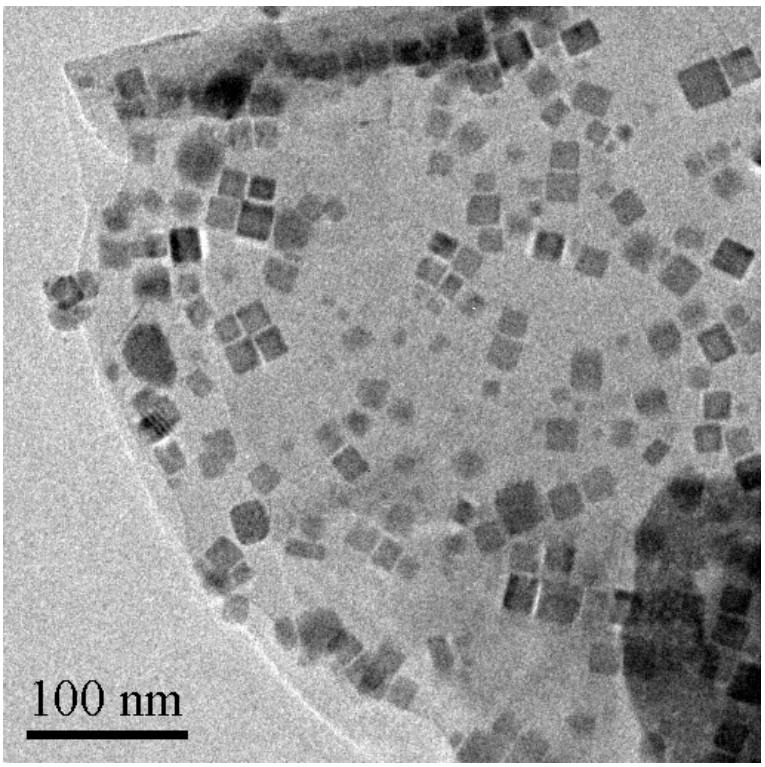

Figure S6. TEM image of CPB@BN-E after ultrasonic treatment with 1 h.

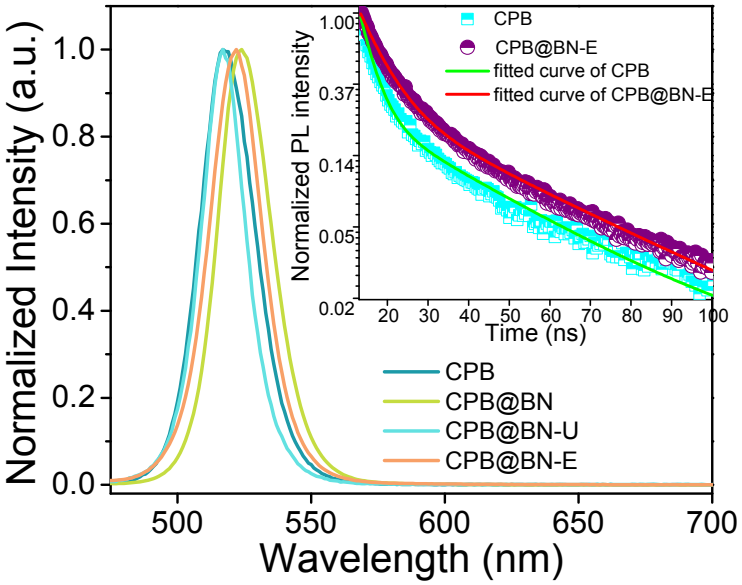

Figure S7. PL spectra of pure CPB NCs, CPB@BN, CPB@BN-E and CPB@BN-U composites. Inset is the PL decay curves of CPB NCs and CPB@BN-E composite.

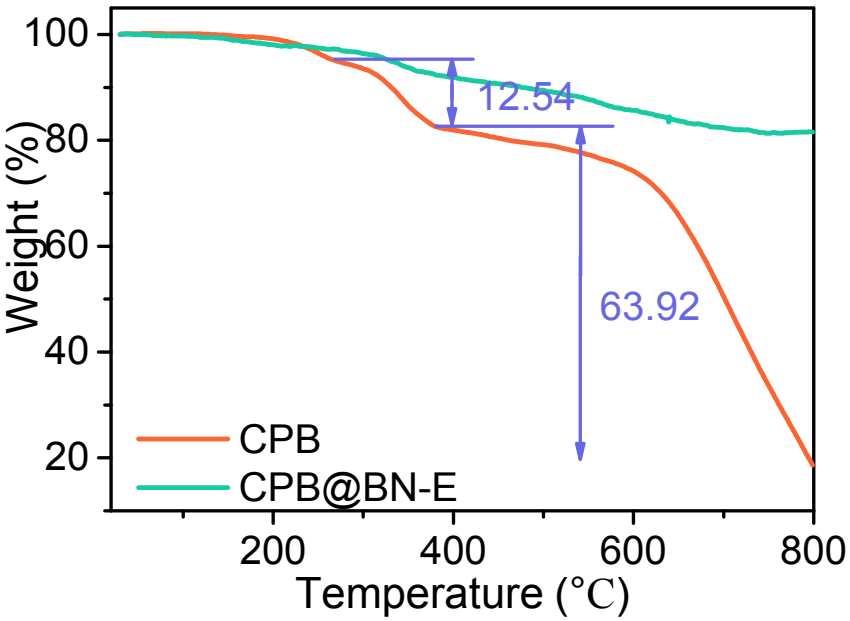

Figure S8. TGA curves of pure CPB NCs and CPB@BN-E composite.

As is shown in Figure S8, the pure CPB NCs present more than 80 wt% weight loss comparing to less than 20 wt% for CPB@BN-E composite at 800°C. The CPB@BN-E composite exhibits a small weight loss centered at around 200°C mainly resulting from the release of absorbed water. The curve of CPB@BN-E composite obviously drops slowly comparing to the pure CPB.

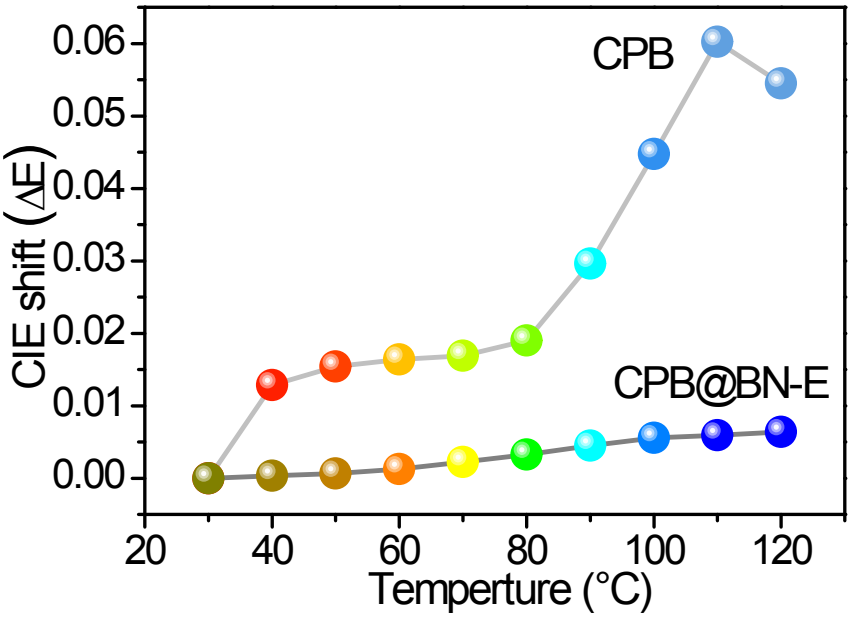

Figure S9. Chromaticity shift of CPB and CPB@BN-E samples as a function of temperature from 30°C to 120°C.

Excellent chromaticity stability is also necessary for phosphor when applying to lighting devices. Therefore, the chromaticity shifts (ΔE) of CPB and CPB@BN-E are assessed using the following equation.[1]

$$\Delta E = \sqrt{(u'_t - u'_0)^2 + (v'_t - v'_0)^2 + (w'_t - w'_0)^2}$$

where u' = 4x/(3 − 2x + 12y), v' = 9y/(3 − 2x + 12y), and w' = 1 − u' − v'. u' and v' are the chromaticity coordinates in u'v' uniform color space, x and y are the chromaticity coordinates in CIE 1931 color space, and 0 and t are the chromaticity shift at 30°C and a given temperature, respectively. By calculating, the ΔE of CPB@BN-E almost remains unchanged with temperature from 30 to 120°C (Figure 3d). However, pure CPB generates an obvious chromaticity shift with the value about 0.055 at 120℃, which is almost 11 times than that of CPB@BN-E. The smaller chromaticity shift means the higher chromaticity stability of CPB@BN-E, which makes it a better application prospect in lighting devices.

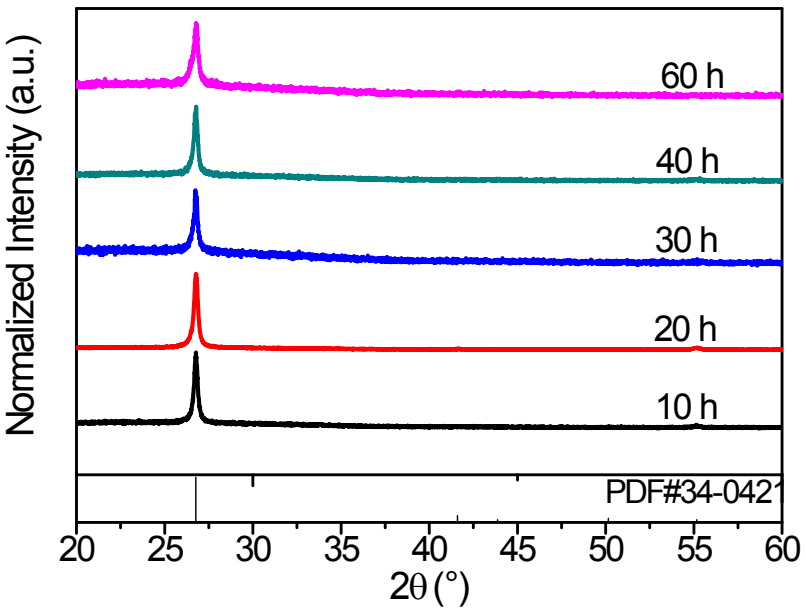

Figure S10. XRD patterns of BN with different exfoliation time. With prolonging the time to 60 h, the peak at 26.8 º changed from sharp and narrow to broader, indicating a smaller size of particle.

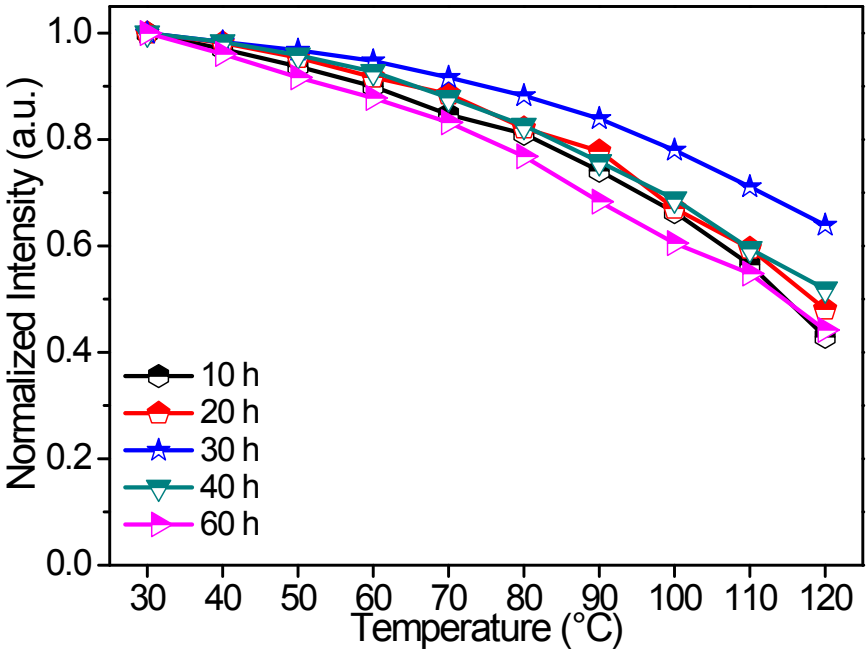

Figure S11. Thermal stability test of CPB@BN-E with different exfoliated time (10 h, 20 h, 30 h, 40 h and 60 h).

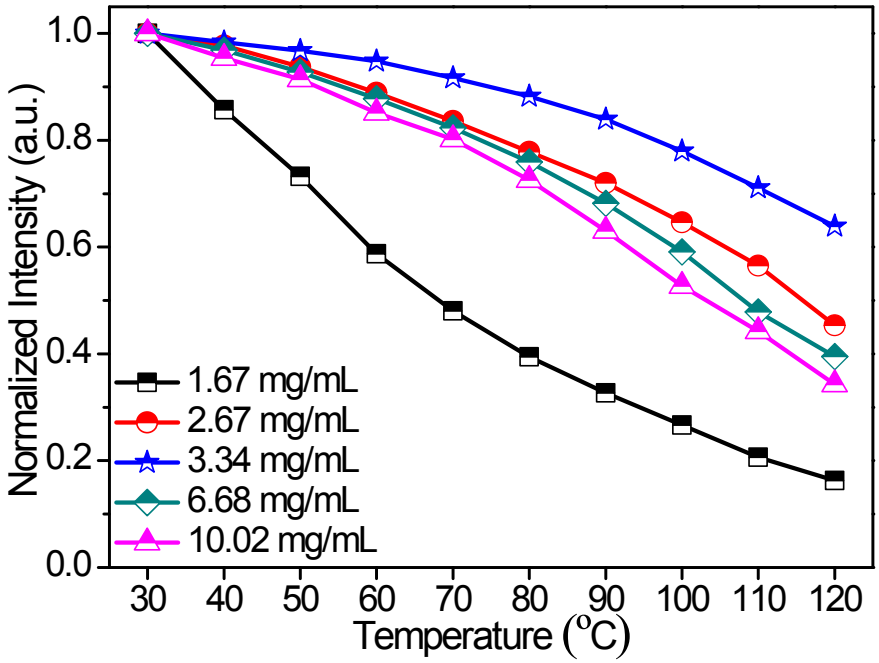

Figure S12. Thermal stability test of CPB@BN-E with changed incorporated BN-E (1.67, 2.67, 3.34, 6.68 and 10.02 mg/mL).

Figure S9 firstly gives the XRD patterns of BN exploited at different times (10 h, 20 h, 30 h, 40 h and 60 h). All exploited h-BN samples show a strong peak at 26.8º responding to (002) plane, which match well with the standard data of BN, implying no structural damage occurs and good crystallinity is reserved. After constructing the CPB@BN-E composites with BN-E at different exploiting time, the thermal stability are compared. As suggested in Figure S10, the thermal stabilities of above CPB@BN-E composites firstly increase along with exploiting time, reaching an optimal value at 30 h, and then drop with prolonging exploiting time. The former increase in thermal stability is mainly attributed to the fact that the smaller particle size of BN-E NSs which enhance the thermal transmission rate. Hence it could be easier to transfer heat from CPB. While the latter decrease should originate from the increase of surface defects with much smaller size of BN, which induces more non-radiation transition.[2,3] When changing the concentration of BN-E in precursor solution (1.67, 2.67, 3.34, 6.68 and 10.02 mg/mL), the corresponding thermal stabilities of as-prepared composite powders present a similar trend to that

changing exfoliating time, which increase at first and then decrease (Figure S11). The optimized volume content of BN-E in CPB@BN-E composites is 3.34 mg/mL.

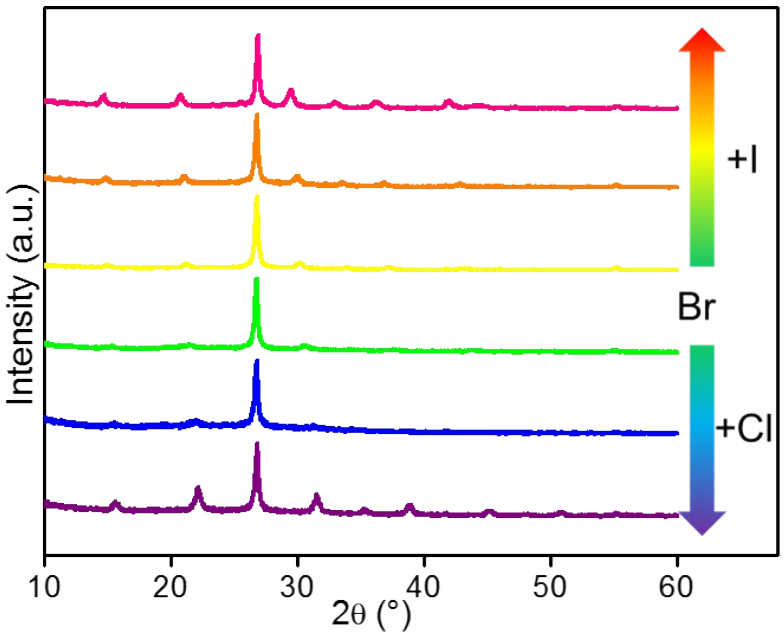

Figure S13. The XRD patterns of perovskite CPX@BN-E composites (X = Cl, Br, I or mixed halide) by changing the halide ion and molar ratio. From bottom to top are $CsPb(Cl_{0.6}Br_{0.4})_3$@BN-E, $CsPb(Cl_{0.5}Br_{0.5})_3$@BN-E, $CsPbBr_3$@BN-E, $CsPb(Br_{0.6}I_{0.4})_3$@BN-E, $CsPb(Br_{0.5}I_{0.5})_3$@BN-E and $CsPb(Br_{0.4}I_{0.6})_3$@BN-E, respectively.

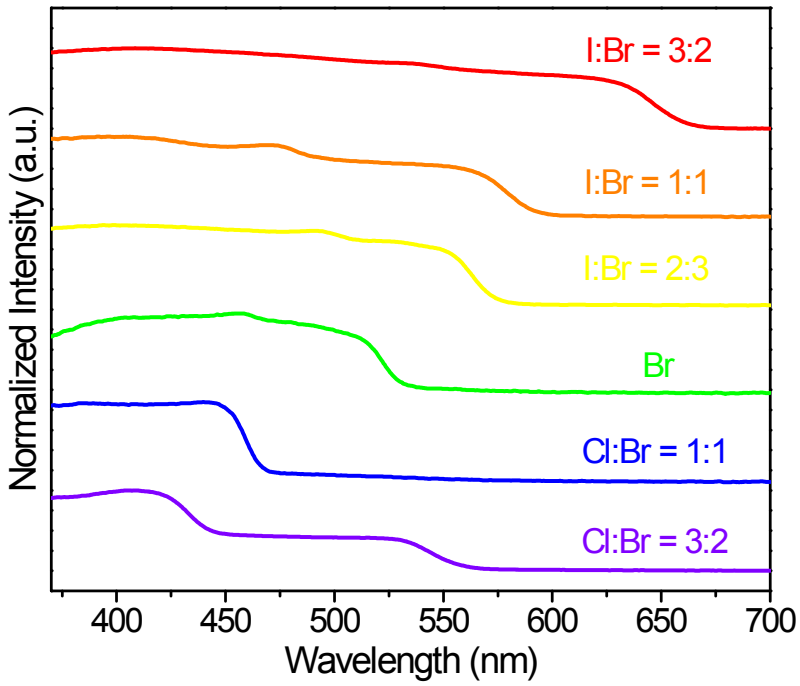

Figure S14. The UV/vis spectra of CPX@BN-E composites.

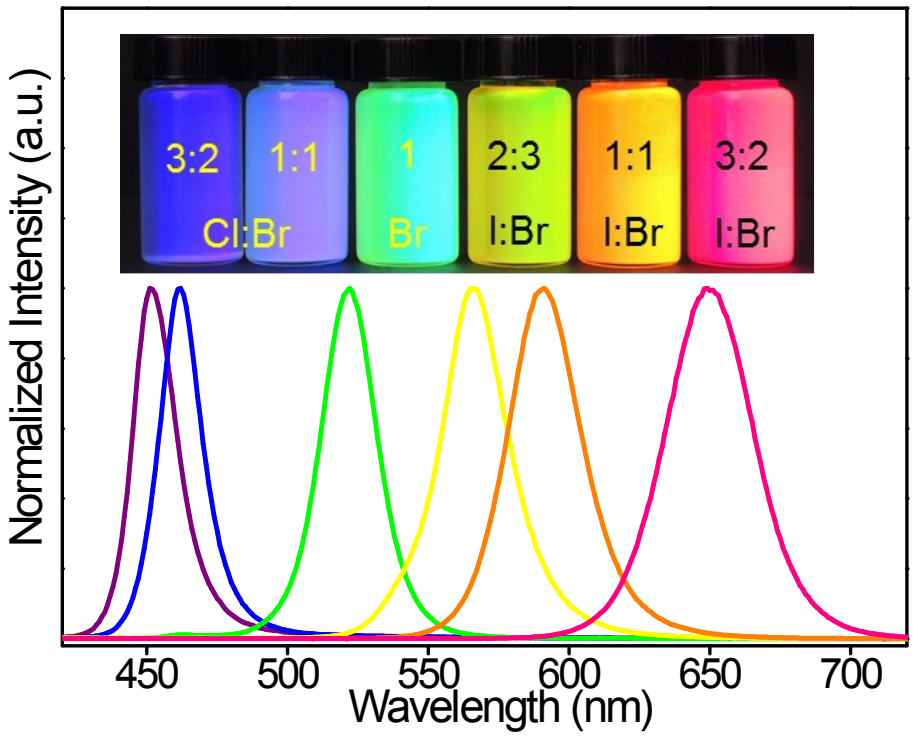

Figure S15. PL spectra of perovskite CPX@BN-E composites (X = Cl, Br, I or mixed halide) by changing the halide ion and molar ratio. From left to right are $CsPb(Cl_{0.6}Br_{0.4})_3$@BN-E, $CsPb(Cl_{0.5}Br_{0.5})_3$@BN-E, $CsPbBr_3$@BN-E, $CsPb(Br_{0.6}I_{0.4})_3$@BN-E, $CsPb(Br_{0.5}I_{0.5})_3$@BN-E and $CsPb(Br_{0.4}I_{0.6})_3$@BN-E, respectively. Inset shows photographs of corresponding samples under UV light (365 nm).

Table S1. Summary of recent passivation studies of CPB NCs for the enhancement of thermal stability.

Refs	Publication year/month	Passivation precursor	Residual intensity at 100 ℃
Wang and co-workers	2016/5	SiO_2	≈ 40%
Yuan and co-workers	2018/5	Glass	≈ 20%
Chen and co-workers	2018/5	Dual-SiO_2	≈ 29%
Hai and co-workers	2017/4	PVP	65%
Lou and co-workers[4]	2017/6	NH_4Br	37%
Yoon and co-workers	2018/5	SiN_xO_y	52%
Li and co-workers	2017/5	SiO_2-Al_2O_3	70%
this report		BN	≈ 85%

Table S2. Thermal conductivity of CPB NCs, BN-E and CPB@BN-E samples.

Samples	Thermal conductivity ($W \cdot m^{-1} \cdot K^{-1}$)		
	CPB	BN-E	CPB@BN-E
1	0.1148	0.1874	0.1747
2	0.1154	0.1872	0.1762
3	0.1155	0.1875	0.1751
4	0.1144	0.1871	0.1774
5	0.1149	0.1872	0.1741
6	0.1150	0.1875	0.1731
7	0.1156	0.1837	0.1669
8	0.1157	0.1875	0.1753
9	0.1157	0.1837	0.1710
10	0.1151	0.1847	0.1776
11	0.1151	0.1882	0.1731
12	0.1155	0.1880	0.1729
13	0.1158	0.1842	0.1751
14	0.1159	0.1880	0.1752
15	0.1157	0.1842	0.1750
16	0.1152	0.1883	0.1760
17	0.1159	0.1882	0.1738
18	0.1148	0.1891	0.1749
19	0.1154	0.1890	0.1759
20	0.1154	0.1885	0.1726
average	0.1153	0.1870	0.1743

References

1 J. Zhou, Z. Xia, M. S. Molokeev, X. Zhang, D. Peng, Q. Liu, *J. Mater. Chem. A* 2017, **5**, 15031-15037.

2 H. C. Wang, Z. Bao, H. Y. Tsai, A. C. Tang, R. S. Liu, *Small* 2018, **14**, 1702433.

3 H. Sun, Z. Yang, M. Wei, W. Sun, X. Li, S. Ye, Y. Zhao, H. Tan, E. L. Kynaston, T. B. Schon, H. Yan, Z. H. Lu, G. A. Ozin, E. H. Sargent, D. S. Seferos, *Adv. Mater.* 2017, **29**, 1701153-1701162.

4 S. Lou, T. Xuan, C. Yu, M. Cao, C. Xia, J. Wang, H. Li, *J. Mater. Chem. C* 2017, **5**, 7431-7435.